Hydrogen Atoms Cause Long-Range Electronic Effects on Graphite

P. Ruffieux,* O. Gröning, P. Schwaller, L. Schlapbach, and P. Gröning

Physics Department, University of Fribourg, Pérolles, CH-1700 Fribourg, Switzerland
(Received 12 November 1999)

We report on long-range electronic effects caused by hydrogen-carbon interaction at the graphite surface. Two types of defects could be distinguished with a combined mode of scanning tunneling microscopy and atomic force microscopy: chemisorption of hydrogen on the basal plane of graphite and atomic vacancy formation. Both types show a $(\sqrt{3} \times \sqrt{3})R30°$ superlattice in the local density of states but have a different topographic structure. The range of modifications in the electronic structure, of fundamental importance for electronic devices based on carbon nanostructures, has been found to be of the order of 20–25 lattice constants.

Defects control many physical properties of solids and dominate the electronic behavior of nanoscale metallic and semiconducting systems, particularly at low dimensions. The study of changes in the electronic structure of graphite due to adsorbates is relevant for other carbon materials (such as nanotubes, fullerenes, etc.) having the six membered ring as a structural unit [1]. Scanning tunneling microscopy (STM) makes it possible to directly investigate the electronic features induced by defects with atomic resolution [2,3]. Graphite was one of the first materials for which long-range order electronic effects caused by surface defects have been predicted and experimentally observed using STM [4,5]. Graphite is a semimetal composed of stacked hexagonal planes of sp^2 hybrid bonded carbon atoms. The *ABAB* stacking of these planes in a three-dimensional crystal creates two inequivalent sites with different properties with regard to the electronic structure: α site atoms are exactly located above atoms of the underlying plane, whereas β site atoms are located above the center of the hexagonal rings of the underlying plane. The weak van der Waals interaction between adjacent planes leads to a suppression of the charge density at the Fermi level at α sites [6]. These two inequivalent sites explain the fact that with STM, which probes only electronic states near the Fermi level, a trigonal symmetry on the graphite surface is imaged.

In this Letter we report on new electronic effects caused by adsorption of atomic hydrogen on graphitic surfaces. A combined mode of STM and atomic force microscopy (AFM) was used to study both topographic and electronic changes in the vicinity of defects. The interaction of an individual H atom with a graphite surface modifies the electronic structure over 20–25 lattice constants leading to a $(\sqrt{3} \times \sqrt{3})R30°$ superstructure in the local density of states (LDOS). A detailed understanding of such defect induced electronic modifications is indispensable for the development of electronic devices based on carbon nanostructures [1,7,8].

Samples of highly oriented pyrolithic graphite were cleaved in air with adhesive tape right before loading into the hydrogen electron cyclotron resonance (ECR) plasma chamber which served as a hydrogen ion source [9]. Typically a gas pressure of 10^{-3} mbar hydrogen was used for the plasma treatment, the base pressure of the chamber being in the low 10^{-8} mbar range. The average ion energy at this pressure is $\sim$10 eV. The sample is set to ground potential. The ion flux at the sample position is typically 10^{12} cm^{-2} s^{-1}. Sample heating can be neglected under these conditions. After plasma treatment, the samples were either vacuum transferred to a connected photoelectron spectrometer (VG ESCALAB 5) equipped with a Mg $K\alpha$ ($h\nu$ = 1253.6 eV) anode for x-ray photoelectron spectroscopy (XPS) and a helium discharge lamp ($h\nu$ = 21.2 eV) for ultraviolet photoelectron spectroscopy (UPS) or transferred in air to an atomic force/scanning tunneling microscope (AFM/STM) (OMICRON) working in ultrahigh vacuum at room temperature. In order to observe isolated defects with scanning probe microscopy short plasma treatment times, typically a few seconds, were used resulting in a defect density of $\sim$10^{-2} nm^{-2}. To overcome the detection limit for the hydrogen induced features in XPS and UPS, however, the sample was treated for 300 s. To obtain the topographic structure around one single defect, the surface was scanned using a conductive cantilever in the AFM contact mode. This has the advantage of simultaneous imaging of the rearrangement of atom positions (AFM signals) and of the affected LDOS (current signal) in the vicinity of a defect. Atomically resolved current and topography images could be obtained using silicon nitride AFM tips coated with highly conductive boron doped diamond. Scan rates and applied forces in the contact mode were typically 10 Hz and 1 nN, respectively. For the simultaneous measurement of the current image a gap voltage of 30–100 mV was applied to the AFM tip.

Simultaneous measurements of the current and AFM signals, such as normal force, lateral force, and the piezo z position, do not only yield the topographic and electronic structure of defects but additionally give information about changes of the tip condition: Sudden changes to higher

tunneling currents for a given force setpoint indicate the sticking of a graphitic flake at the AFM tip.

Scanning the plasma treated surface with a conventional STM tip (W) revealed the well-known protrusions around the adsorption sites [4]. However, imaging the same surface in AFM mode did not show any elevated structures at the adsorption site. To understand these at first sight contradictory results, it should be kept in mind that STM probes the occupied or unoccupied (depending on the sign of the sample bias) LDOS near the Fermi energy whereas AFM probes the total charge density. In the following, we describe the two types of defects we observed, namely, chemisorbed hydrogen and atomic vacancies.

Chemisorbed hydrogen: Scanning the plasma treated surface in the AFM contact mode with simultaneous acquisition of the current signal yields clear superlattice-type modifications of the electronic properties over a distance
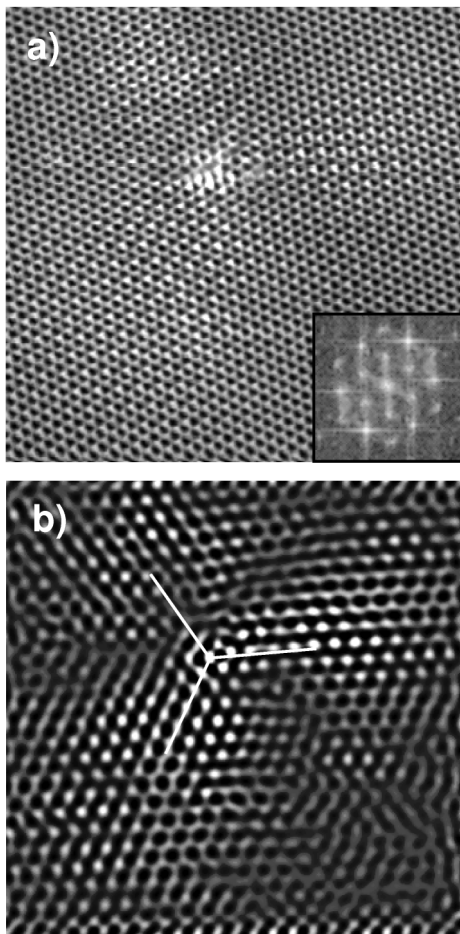
FIG. 1. (a) Current image of a hydrogen plasma treated graphite surface recorded in AFM contact mode (94 Å × 94 Å). Measurement parameters are as follows: force setpoint: 2 nN, sample bias: 30 mV. Current range: 1 nA (black)–9 nA (white). The inset shows the center of the FFT of (a). (b) The same data as (a) after applying a two-dimensional bandpass filter to isolate the superlattice component.

of 25 lattice constants (Fig. 1). However, no modifications were detected in the topography image. In the inset of Fig. 1(a), the center of the fast Fourier transform (FFT) of the current image is displayed. The six inner spots correspond to the $(\sqrt{3} \times \sqrt{3})R30°$ superstructure. The six outer spots with the same orientation are due to the second harmonic of the superlattice, whereas the six outer spots rotated by 30° originate from the regular graphite lattice, i.e., the imaging of the β site atoms. The scattering pattern is independent of the applied sample bias (30–100 mV) for both, tunneling from occupied states and tunneling into unoccupied states of the sample. The threefold symmetry of the scattering pattern is clearly seen in Fig. 1(b), which shows the same data as 1(a) but after applying a two-dimensional bandpass filter to isolate the superlattice contribution. The scattering pattern has the same orientation as the superstructure, which is indicated by the lines in Fig. 1(b). Applying the bandpass filter to the six spots originating from the regular graphite lattice does not reveal any threefold scattering pattern.

Kelly et al. [10] discussed in a recent work the dependence of the orientation of the threefold scattering pattern on the type of atom, which is affected by an atomic vacancy. Scattering patterns originating from α site defects are rotated by 60° relative to the ones from β site atoms reflecting the symmetry of the dangling bonds of the nearest neighbors. These bonds are also affected if the hybridization of a carbon atom is changed by forming an additional bond to an adsorbed hydrogen atom. The lack of topographic modifications and the results of photoelectron spectroscopy (see below) suggest that this type of defect is caused by chemisorbed hydrogen atoms. Only one type of carbon atom seems to be affected. If α and β sites were involved, one would expect a sixfold symmetric scattering pattern.

A more detailed analysis of the bandpass filtered current image shows that the measured scattering pattern results from two interfering scattering patterns with the same orientation, but with an origin shift of 2.46 Å, i.e., the distance between two carbon atoms of the same type. The range of the superlattice in the electronic structure is found to be of the order of 25 lattice distances. Chen et al. [11] found the chemisorption of hydrogen on the basal plane of graphite to be endothermic. A metastable state exists in all examined configurations, the most stable one being the on-top site. The on-top configuration also shows the lowest activation barrier ($\sim$1.8 eV). In an ECR plasma the ion energy (typically 10 eV) is large enough to populate this state, in contrast to treatments with an atomic hydrogen source [12], where we could not detect any adsorption of hydrogen on the basal plane of graphite.

Figure 2(a) shows normal emission photoelectron spectra recorded from the graphite surface before and after the hydrogen plasma treatment. In order to be able to determine the work function ϕ of the surface, we applied a sample bias of -10 V. The cutoff at low kinetic energies
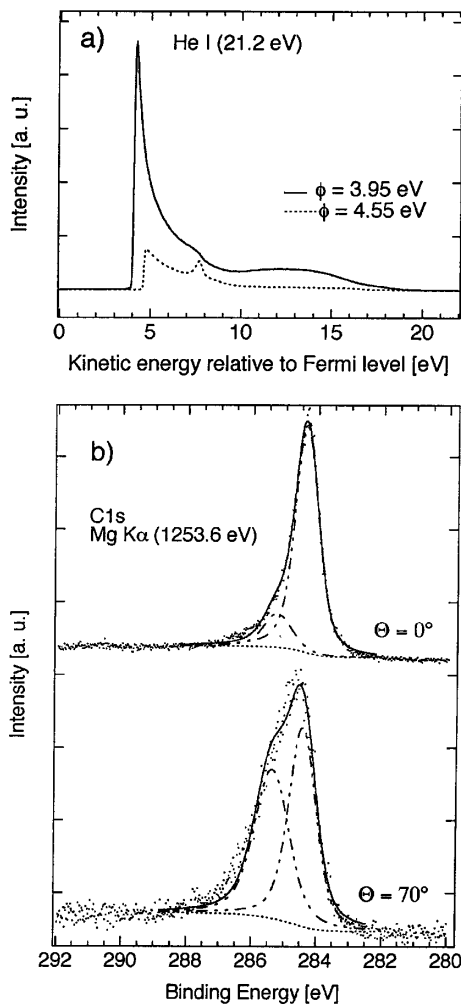
FIG. 2.   (a) Normal emission He I spectra before and after hydrogen plasma treatment. Sample bias: −10 V. (b) C $1s$ core level spectra of the hydrogen plasma treated graphite for normal (top) and grazing emission (bottom).

reveals that the work function of the treated surface is lowered by 0.6 eV relative to that of the untreated surface. The lower work function indicates a change in the surface dipole moment originating from the polarized C-H bond. Since carbon is the more electronegative element, hydrogen atoms have to be positioned above the carbon atoms of the first monolayer. A lowering of the work function has also been observed for diamond where the hydrogen saturated surface has negative electron affinity [13–15]. The origin of this new dipole moment can be detected with XPS. Figure 2(b) shows C $1s$ core level photoelectron spectra of the treated graphite surface for normal (top) and grazing emission (enhanced surface sensitivity). Analysis of relative intensities for different emission angles show that the hydrogen plasma induced feature at higher binding energy (285.4 eV) originates from the surface. A shift of 1.0 eV relative to the bulk contribution has also been observed on the hydrogen terminated diamond surface [13,16]. It has been shown for

different carbon systems that, although carbon is the more electronegative element, the C-H contribution appears at higher binding energies. This has to be explained rather by a different relaxation energy (final state) for the differently hybridized carbon atoms of the first monolayer than simply with a Koopman's shift (initial state) [16–18].

Atomic vacancies: Typical images of the simultaneously recorded current and topography images of a local defect are shown in Fig. 3. The topographic structure of this defect consists of three local depressions with a corrugation of 0.3 Å. This strong enhancement of the corrugation, as compared to the 10 times weaker corrugation of defect-free zones, is interpreted as atomic vacancies in the first carbon monolayer, which were formed upon the hydrogen plasma treatment. The vacancy formation probability is found to be 5 times smaller than hydrogen adsorption. The depressions in Fig. 3(b) are separated by 4.1 Å. The direction and the distance between the topographic minima show that carbon atoms of the same type are affected (distance between second nearest neighbors of the same type is $\sqrt{3} \times 2.46$ Å $= 4.26$ Å). The current image shows the enhanced LDOS in the vicinity of the defect and again the $(\sqrt{3} \times \sqrt{3})R30°$ superlattice, which is visible over 25 lattice constants. The calculated LDOS for a single atomic vacancy [4] [Fig. 3(c)] shows the same features as we find for defects showing depressions in the topography image.
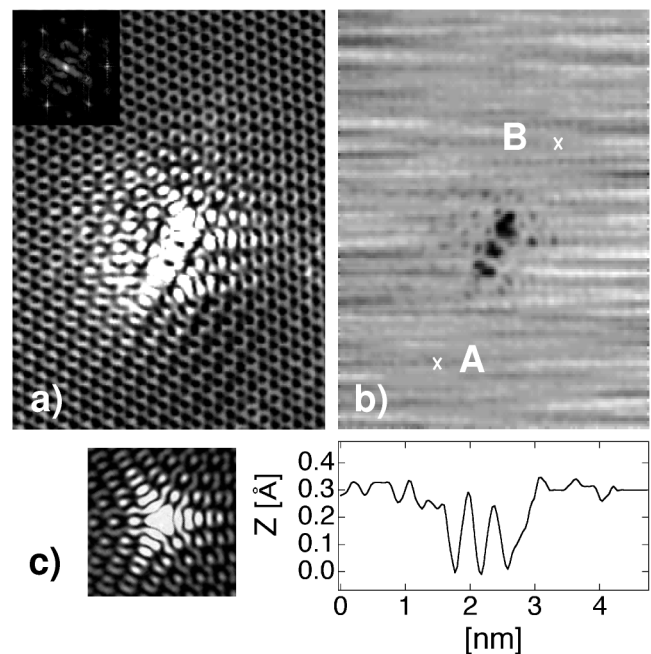
FIG. 3.   Simultaneously recorded current and topography image of a hydrogen plasma treated graphite surface in AFM contact mode (58 Å × 78 Å). Measurement parameters: force setpoint: 2 nN; sample bias: 30 mV. (a) Current image with FFT (inset). Current range: 2 nA (black)−40 nA (white). (b) Topography image with line profile from A to B. (c) Calculated LDOS in the vicinity of a single atomic vacancy using a tight binding model (reprinted with permission from [4]).

The threshold energies for sputtering off carbon atoms has been calculated by Bohdansky and Roth [19]. For a target-to-projectile ratio of $M_2/M_1 \leq 0.3$, the threshold energy is given by the empirical relation $E_{th} = \frac{U_0}{\gamma(1-\gamma)}$, where U_0 is the binding energy of surface atoms, and $\gamma = 4\frac{M_1M_2}{(M_1+M_2)^2}$ is the energy transfer coefficient. For the interaction of hydrogen ions with graphite an energy threshold of $E_{th} \simeq 36$ eV (where U_0 can be approximated by the heat of sublimation [19]: $U_0 \simeq 7.4$ eV [20]) results from these considerations. The maximum ion energy in ECR plasma treatments is given by the plasma potential which originates from the different mobilities of electrons and ions. The potential depends on the chamber geometry and the gas pressure. The maximum ion energies in the plasma chamber used for this experiment range from ~ 22 eV (10^{-4} mbar) to about 9 eV (10^{-1} mbar) [9] which is well below the estimated energy threshold for vacancy formation by sputtering. A possible channel for vacancy formation is the neutralization process of the ions. The charge transfer from the surface to the approaching ion leads to a weakening and a finite destruction cross section of the sp^2 bonds [21].

In summary, our studies of the interaction of hydrogen ions with the graphite surface by means of a combined mode of AFM/STM and photoelectron spectroscopy reveal chemisorption of hydrogen and atomic vacancy formation on the basal plane of graphite. Chemisorbed hydrogen does not show any structure in the topography signal but consists of a local charge enhancement and a long-range perturbation of the electronic structure consisting of a $(\sqrt{3} \times \sqrt{3})R30°$ superstructure in the LDOS. The range of the modified electronic structure is of the order of 6 nm. Atomic vacancies consist of local depressions in the topography image. The current image of this defect type shows a local charge enhancement, which is in good agreement with the previously calculated LDOS near an atomic vacancy and again a $(\sqrt{3} \times \sqrt{3})R30°$ superlattice in the vicinity of the defect. Simultaneous recording of topography and current signal in the AFM contact mode has been found to be a powerful tool for imaging both the topographic structure and the long-range changes in the LDOS of defects.

*Corresponding author.
Electronic address: pascal.ruffieux@unifr.ch

[1] M. S. Dresselhaus, G. Dresselhaus, and P. C. Eklund, *Science of Fullerenes and Carbon Nanotubes* (Academic Press, San Diego, 1996).

[2] M. F. Crommie, C. P. Lutz, and D. M. Eigler, Nature (London) **363**, 524 (1993).

[3] Y. Hasegawa and Ph. Avouris, Phys. Rev. Lett. **71**, 1071 (1993).

[4] H. A. Mizes and J. S. Foster, Science **244**, 559 (1989).

[5] J. Xhie, K. Sattler, U. Muller, N. Venkateswaran, and G. Raina, Phys. Rev. B **43**, 8917 (1991).

[6] D. Tomanek, S. G. Louie, H. J. Mamin, D. W. Abraham, R. E. Thomson, E. Ganz, and J. Clarke, Phys. Rev. B **35**, 7790 (1987).

[7] L. C. Venema, J. W. G. Wildóer, J. W. Janssen, S. J. Tans, H. L. J. Temminck Tuinstra, L. P. Kouwenhoven, and C. Dekker, Science **283**, 52 (1999).

[8] F. Léonard and J. Tersoff, Phys. Rev. Lett. **83**, 5174 (1999).

[9] S. Nowak, P. Gröning, O. M. Küttel, M. Collaud, and G. Dietler, J. Vac. Sci. Technol. A **10**, 3419 (1992).

[10] K. F. Kelly and N. J. Halas, Surf. Sci. **416**, L1085 (1998).

[11] J. P. Chen and R. T. Yang, Surf. Sci. **216**, 481 (1989).

[12] U. Bischler and E. Bertel, J. Vac. Sci. Technol. A **11**, 458 (1993).

[13] L. Diederich, O. M. Küttel, P. Aebi, and L. Schlapbach, Surf. Sci. **418**, 219 (1998).

[14] F. J. Himpsel, J. A. Knapp, J. A. VanVechten, and D. E. Eastman, Phys. Rev. B **20**, 624 (1979).

[15] J. B. Cui, J. Ristein, and L. Ley, Phys. Rev. Lett. **81**, 429 (1998).

[16] R. Graupner, Ph.D. thesis, University of Erlangen-Nürnberg, 1997.

[17] J. J. Pireaux, S. Svensson, E. Basilier, P.-A. Malmqvist, U. Gelius, R. Caudano, and K. Siegmann, Phys. Rev. A **14**, 2133 (1976).

[18] G. Beamson and D. Briggs, *High Resolution XPS of Organic Polymers* (Wiley, Chichester, 1992).

[19] J. Bohdansky and J. Roth, J. Appl. Phys. **51**, 2861 (1980).

[20] B. T. Kelly, *Physics of Graphite* (Applied Science Publishers, New Jersey, 1981).

[21] V. V. Khvostov, M. B. Guseva, V. G. Babaev, and E. A. Osherovich, Surf. Sci. **320**, L123 (1994).